RSC Advances

ROYAL SOCIETY OF CHEMISTRY

www.rsc.org/advances

Studies of dispersed liquid crystals in binary mixtures with ionic liquid and their excitation by electric signals

Jagdeesh Kumar Srivastava,[a] Rajendra Kumar Singh,[a] Ravindra Dhar[b] and Shri Singh[a*]

[a] *Department of Physics, Banaras Hindu University, Varanasi, India*

[b] *Centre of Material Sciences, University of Allahabad, Allahabad, India*

We report the results of dispersion studies of two nematogens (i) 6CHBT (4-(*trans*-4-*n*-hexylcyclohexyl)isothiocyanatobenzene) and (ii) PCH5 (4-(trans-4-pentyl-cyclohexyl) benzonitrile) in their binary mixtures with phosphonium based ionic liquid $[P_{6,6,6,14}][Ntf_2]$ (trihexyl(tetradecyl)phosphoniumbis(trifluoromethylsulfonyl)amide). The morphology and properties of these mixtures have been investigated by using differential scanning calorimetry (DSC), polarizing optical microscopy (POM), Fourier transform infrared spectroscopy (FTIR), thermogravimetric analysis(TGA), and, their excitations by electric signals. For both the liquid crystals, nematic droplets are found to be dispersed in the ionic liquid having a particular anion, i.e., $[Ntf_2]$. These droplets resemble closely with the common droplet morphologies observed in polymer dispersed liquid crystals. Thermal and morphological investigations on the mixtures show decrease in the peak value of isotropic to nematic transition and broadening of the associated peak with decrease in the compositions of nematogens in mixtures. As a result, nematic droplets in a wide temperature range ~20 ^{0}C (i.e., from ~ 16 ^{0}C to ~ 36 ^{0}C) are observed for various mixtures. Electrical excitations of the mixtures show significant changes in the droplet size and nematic director orientation inside the droplets due to change in the anchoring conditions with the application of external electric pulses. Influence of the electric field on these nematic droplets and their stability over a wide temperature range suggests its potential for various device development applications.

KEYWORDS: Liquid crystals, Ionic liquids, Dispersion studies, Nematic droplets

*Corresponding author. Email: srisingh23@gmail.com, Ph : +91 9935025416
Fax : +91 542 2368390

Introduction

Liquid crystal (LC) dispersion has been the subject of considerable interest in the field of soft condensed state, and during past two decades much attention has been paid on investigating its

behaviour from the point of view of basic understanding and applications.[1–5] One of the main outcomes of these dispersion studies results in the form of polymer dispersed liquid crystals (PDLCs).[6,7] It is useful not only in various device development applications[1,2] but also in addressing the fundamental questions related with the phase separation,[3] director configurations in confined geometries,[4] electro – optical properties,[5] etc. The most common studies on PDLCs have been focused to improve its electro – optical and morphological properties,[8,9] droplet size,[10–13] phase diagram and miscibility behaviour,[14-16,] etc. Attention is being paid to continue the work with the use of different polymeric substrates,[17,18] multicolour PDLCs,[19] photo alignment techniques,[20] self – assembling of LCs[10,21,22] and synthesis of ionic liquid crystals (ILCs) having various mesophases.[23-25]

The phase segregation and self – assembling using partially incompatible molecules provide additional functionality such as ionic conductivity to these materials.[22] Nematic, being the least ordered and viscous among the various mesophases can be realigned under external stimulation more easily as compared with other mesophases.[25] Such materials have also found applications in ion transport,[25] smart windows,[26] reverse mode PDLCs,[27,28] etc. Dielectric force induced LC alignment and interfacial deformation inside the LC droplets have been also the subject of considerable interest.[29,30] Alignment of the LC molecules can also be controlled internally by the weak intermolecular interactions such as hydrogen bonding and ionic interactions using some partially incompatible ionic molecules.[23,24] This may also enhance the ionic conductivity of the mixtures as well. Therefore, ionic liquid crystals with nematic phase or nematic liquid crystals with ionic properties may provide new scopes for the technological improvements.

Motivation to the present work originates from the fact that inspite of extensive studies on ionic liquid crystals having various mesophases[23,24] there are only sporadic studies on the ionic liquid crystals exhibiting nematic phase near room temperature[25,31,32]. It is obvious because most of the ILCs consist of a single ionic head group involving linear molecules which is connected with one or multiple long aliphatic tails. The micro-segregation of incompatible units, aggregation of compatible units and minimization of volume results generally in the lamellar or columnar phases at higher temperatures.[23-25] Being difficulties in having nematogenic ILCs, our curiosity is to inspect the changes occurring in the droplet morphologies and LC director orientations inside these droplets in the well explored nematogenic compounds, when an ionic flavor is added to their mixtures. With the addition of ionic moieties in these mixtures, even a small change in the externally applied electric field or pulse width is supposed to make significant influence on the LC director orientation and droplet morphology due to sufficient swift in anchoring conditions near isotropic to nematic phase transition temperature.[33,34]

For the said purpose, we focused our attention on two nematogens 6CHBT and PCH5 which show the co-existence of isotropic to nematic transition *via 'droplets'* in their mixtures with other solvents.[33-36] In the present study, binary mixtures of these two nematogens with phosphonium ionic liquid i.e., $[P_{6,6,6,14}][Ntf_2]$ have been used to obtain the phase separated LC droplets having a close resemblance with the droplets found in conventional PDLCs. Materials and methodologies used for the preparation and investigation of the various binary mixtures have been discussed in experimental section. The result and discussion section concerns with the thermal and morphological investigations, effect of varying field strength on LC droplets and their director orientation, thermal stability and interaction behaviour of LCs and IL. Paper ends with the summary and conclusion in the last section.

Experimental

Materials

For the preparation of various binary mixtures both nematogens and ionic liquid were procured from Sigma-Aldrich which were of the highest available purity and used without further purification. The liquid crystals 6CHBT (i.e., 4-(*trans*-4-*n*-hexylcyclohexyl)isothiocyanato benzene) and PCH5 (i.e., 4-(trans-4-pentyl-cyclo hexyl) benzonitrile) have 99% purity, whereas, the purity of ionic liquid $[P_{6,6,6,14}][Ntf_2]$ (i.e., (trihexyl(tetradecyl)phosphonium bis (trifluoro methylsulfonyl) amide) is 95%. To remove the volatile impurities from the ionic liquid it is dried in vacuum (at $\sim 10^{-3}$ Torr) for 24 hours before using it in mixtures. We have chosen these nematogens on the basis of some earlier studies related with the coexistence of isotropic and nematic (*IN*) regions in their mixtures with other solvents.[33,34] The 6CHBT is a widely studied NLC which shows *nematic droplets* in coexistence with isotropic regions of phenyl isocyanate[33] and benzene.[34] Another NLC, PCH5 had also been well studied and shows dynamics very similar to 6CHBT in nematic phase.[35,36] The phosphonium ionic liquid (PIL) with $[Ntf_2]$ anion has been used in the present investigation due to its special property of forming matrix with low glass transition temperature and preferential interaction between $[Ntf_2]$ anion and phosphonium cation.[37] Studies on these materials motivated us to use them in our present work for preparing binary mixtures where phase separated nematic droplets can also be observed.

Methodologies

The binary mixtures have been prepared by stirring different compositions of nematogens and PIL at 120 ^{0}C for about three hours. Measurements were carried out after keeping the mixtures at room temperature for more than 72 hours so that the stability of the mixtures can be ensured. The abbreviations used for various binary mixtures in the text are given in **Table 1**.

Thermal studies of the mixtures have been carried out using differential scanning calorimeter (Mettler Toledo DSC 1) at scanning rate of 10 ^{0}C/min with continuous purging of N_2 gas at a rate ~30 ml/min. The phase transition temperatures have been measured with temperature accuracy and precision at ± 0.2 K and ± 0.02 K, respectively, and the transition enthalpy with an accuracy of 1%. In order to ensure complete stability of the mixtures and removing moisture, the DSC measurements were performed for two heating – cooling cycles in the temperature range of -40 ^{0}C to 120 ^{0}C with a hold of 10 minute at 120 ^{0}C during the first step. Thermal analyses of these mixtures have been made for the second cooling step.

Morphological investigation of various binary mixtures were carried out after filling them in ITO coated glass cells of thickness 25 μm by capillary action method in their isotropic liquid state at temperature ~35^{0}C. These cells are sealed immediately by an adhesive to avoid air bubbles and then subjected to polarizing optical microscope Leitz DMR POM at 100X magnification for further investigation. For controlled temperature operations, homemade water – bath and sample holder with PID temperature controller having accuracy 0.1^{0}C were used. Effect of the electric field on LC droplets and LC director orientation inside the droplets were studied by applying rectangular electric pulses to these cells through a multifunction generator. Rectangular electric pulses with varying amplitudes (2, 3, 4, 5, and 6V) and three different pulse widths in the ratios 1:4, 1:1 and 4:1, i.e., the pulses having duty cycles 20%, 50% and 80%, respectively, have been used.

For studying the probable interaction and shift in the characteristic vibrations as a result of binary mixings of nematogens and PIL, Perkin Elmer FTIR 1 spectrometer with 0.5 cm^{-1} resolution was employed. The Fourier transform infrared (FTIR) spectra of the mixtures were recorded by wetting KBr pellets with a tiny drop of the mixture.

Mettler Toledo TGA/DSC 1 having accuracy of ±0.3 K was used to study the decomposition temperatures and thermal stability of the mixtures. For studying decomposition behavior, thermogravimetric analyses (TGA) were carried out after keeping the mixtures in alumina pans under N_2 atmosphere and heating them in the temperature range 30 ^{0}C to 600 ^{0}C at scanning rate of 10 ^{0}C/min.

Results and discussion

Thermal investigations

The DSC thermograms for various binary mixtures of both the nematogens and **IL** under second cooling steps are shown in **Fig. 1** and their thermal properties are given in **Table 2**. As compared with isotropic – nematic transition temperature (T_{IN}) of pure **LC$_1$** (T_{IN} = 41.6 ^{0}C), its mixture with **IL** shows remarkable decrease in T_{IN} of **LC$_1$** (**Fig. 1a**). For **ILLC$_1$(50),** observed decrease is 7.5 ^{0}C (in this case, T_{IN} =34.1 ^{0}C). DSC thermograms show that with the decrease in the composition of **LC$_1$** in various mixtures not only the onset and endset of transitions decrease but also result in the broadening of the peak (ΔT) associated with *IN* transition. At full width half maxima, ΔT = 1.3 ^{0}C for **LC$_1$**, whereas, it is 2.9 ^{0}C in the case of **ILLC$_1$(75)**. This broadening can be visualized more clearly on zooming the DSC thermograms for *IN* transition region and is shown in the inset of **Fig. 1a**. It is observed that the nematic phase spreads in a much wider temperature range in their binary mixtures as compared with pure **LC$_1$**.

For cooling at temperatures below 10 ^{0}C, DSC thermograms show double crystallization peaks for **LC$_1$** and multiple crystallization peaks for its various mixtures. This double crystallization peak is due to very complex nature of **LC$_1$** i.e., 6CHBT and is reported to get influenced by thermal history (i.e. the starting temperature) and operating conditions in a DSC experiment.[38,39] Witko et. al.,[39] have suggested that the structural interaction between 6CHBT

molecules should exhibit two distinct and energetically separated modes with its peculiar temperature dependency. Later, it has also been shown that the bulk 6CHBT exhibits several energetically stable and unstable conformers with head-to-head configuration being energetically most favorable one.[38] This structural complexity in the bulk 6CHBT is the main reasons for occurrence of double crystallization peaks in the DSC thermograms at temperatures below 10 ^{0}C.[38] Occurrence of multiple melting and (or) crystallization peaks at lower temperature in the DSC thermograms of these mixtures may be associated with the initial melting and then re-crystallization of the melted mixtures at lower temperature during the process of thermal scanning. Our thought is based on the generalization of the earlier works describing the multiple melting phenomena in 6CHBT[39] and work done by Shuren et. al.,[40] on nylon 1010. It describes the phenomenon of multiple melting as a continuously occurring process of melting and re-crystallization during thermal scanning of the material. Occurrence of an exothermic peak (as a valley) between two endothermic peaks during heating scan is a confirmation for re-crystallization.[40]

Thermal investigation of pure **LC_2** i.e., PCH5 shows single and sharp crystallization peak at lower temperature which gets broadened for the mixtures with smaller content of **IL (Fig. 1b)**. As shown in the inset of **Fig. 1b** only one broad crystallization peak is found for **$ILLC_2$(90)** and **$ILLC_2$(80)** but multiple crystallization peaks occur for comparatively higher contents of **IL** in the mixtures. It is also interesting to note that for intermediate compositions maxima of the crystallization peak occur at temperatures slightly higher than that of pure **LC_2** (**Fig. 1b**) while a shift to lower values in the maxima of the crystallization peak is observed for relatively higher **IL** content in the mixtures i.e., for **$ILLC_2$(60)** and **$ILLC_2$(50)**. Moreover, in these mixtures onset of multiple crystallization occur at temperatures slightly higher than the onset of single

crystallization temperature found in pure **LC_2**. It might be due to freezing / crystallization of pure **IL** at temperatures relatively higher than the crystallization temperatures of pure **LC_2**. Findings are similar to the one observed for binary mixtures of **LC_1** and **IL** where multiple crystallization peak dominates over the double crystallization peak of pure **LC_1** with increasing **IL** content in the mixtures (**Fig. 1a**). Since **IL** shows similar crystallization behavior with both the nematogens in their mixtures at higher **IL** contents, multiple crystallization peaks in these mixtures may result as a combined effect of both the constituents i.e., **LC** and **IL**.

In the region of *IN* transition various binary mixtures of **LC_2** and **IL** show a drastic decrease in T_{IN} for decreasing content of **LC_2** in their mixtures with **IL** (**Fig. 1b**). For **$ILLC_2$(90)** and **$ILLC_2$(80)**, T_{IN} is ~36.7 ^{0}C and ~19.9 ^{0}C, respectively, which is much lower than T_{IN} =55.3 ^{0}C for pure **LC_2**. Moreover, like **LC_1**, for mixtures with **LC_2** we find a significant increase in the range of nematic transition temperature. For pure **LC_2**, ΔT =1.2 ^{0}C, whereas, for **$ILLC_2$(90)** and **$ILLC_2$(80)** the ΔT values are 8.4 ^{0}C and 3.4 ^{0}C, respectively.

Morphological investigations

For various binary mixtures, morphological studies are made in two steps. Initially, LC droplets are studied during cooling of the mixtures (in ITO coated glass cells) from an already heated isotropic state. In the next step cells are subjected to rectangular electric pulses for studying the effect of electric field strength on the LC droplet formation and change in the LC director orientation inside these droplets.

LC droplets morphology

Results of morphological studies for various mixtures of **LC_1** and **IL** are shown in **Fig. 2**. For **$ILLC_1$(90), Fig. 2a** shows two distinct regions with the occurrence of (i) schlieren texture in the broad nematic (i.e. an LC rich) domain and (ii) nematic droplets of different sizes in an IL

rich domain. Similar observations have also been made for **ILLC$_1$(80).** At lower concentrations of **LC$_1$** in the mixtures morphological investigations show only the nematic droplets (and not the broad nematic domains) distributed almost uniformly over the entire area of the cell. Sizes of these nematic droplets decrease with decrease in the concentration of **LC$_1$** in various mixtures. **Figure 2b,c** show the observed decrease in the size of nematic droplets for the two mixtures **ILLC$_1$(75)** and **ILLC$_1$(60)** at 28 ^{0}C. A much larger decrease in the droplet size and T_{IN} is found for **ILLC$_1$(50)** (**Fig. 2d**). In this case, POM images show only tiny nematic droplets at comparatively much lower temperatures (~20 ^{0}C). For all these mixtures, stable nematic droplets occur at temperatures upto ~20 ^{0}C as observed through POM. On further cooling, slight increase in the droplet size is observed due to coalescence of smaller droplets into the larger one. Freezing of nematic droplets in IL rich domains is also observed for temperatures below 10 ^{0}C.

The binary mixing of **LC$_2$** and **IL** also shows the similar behaviour. But, in this case, a large decrease in the *IN* transition temperatures is observed for decreasing content of **LC$_2$** in **IL**. Temperature dependent morphological investigations for **ILLC$_2$(90)** are shown in **Fig. 3**. From POM, it was observed that cooling from an isotropic state at ~50 ^{0}C, formation of tiny nematic droplets starts at ~ 44 ^{0}C and it covers the entire region at ~40 ^{0}C (**Fig. 3a**). Cooling of the mixtures to further lower temperature show coalescence of tiny nematic droplets into a larger one (**Fig. 3b–e**). Coalescence of smaller nematic droplets results in the macroscopic nematic domains with well defined schlieren textures at ~28 ^{0}C (**Fig. 3f**). These observations are similar to the one discussed earlier for **LC$_1$** content above 80 wt% in **IL** (**Fig. 2a**). For both the nematogens (i.e., 6CHBT and PCH5) uniform nematic droplets with decrease in the droplet size have been observed for decreasing content of **LCs** below 80 wt%. Uniformity in the droplet size is maintained due to the formation of tiny droplets at temperatures just below the isotropic state.

These tiny droplets get attached with the surface of the substrate (glass) where relatively strong surface anchoring prevents further coalescence among these droplets.

Figure 4 shows the POM images for two different composition of **LC_2** (i.e., 80% and 75%) in **IL**. It shows decrease in both (i) the droplet size and (ii) the temperature, where, stable and nearly uniform nematic droplets were formed with decrease in the concentration of **LC_2**. For **$ILLC_2$(80)** starting from the isotropic phase at ~35 ^{0}C, formation of tiny nematic droplet starts at ~32^{0}C. **Figure 4a** shows the nematic droplets covering the entire area of the cell at 28 ^{0}C and it remains stable upto temperature ~16 ^{0}C. At further cooling freezing of these droplets in the IL rich phase occurs with an opaque appearance at temperature below 10 ^{0}C (**Fig. 4b**). Change in the droplet size during heating from an already freeze state to the temperature 28 ^{0}C is shown in **Fig. 4c**. Similar results were also observed for **$ILLC_2$(75)** with slight decrease in the droplet size with composition (**Fig. 4d–f**). Moreover, from the DSC investigations of **$ILLC_2$(60)** and **$ILLC_2$(50)**, phase changes are found at much lower temperatures. In this case, any specific information about the nature of the phase transition cannot be inferred through POM due to freezing of the mixtures at an earlier temperature (~10 ^{0}C).

Electrical excitations of LC droplets

Morphological investigations of various binary mixtures under changing electric field strengths show that the size of the nematic droplets and LC director orientation inside the droplets can be tuned by the application of electric signals of different field strengths. Throughout the studies, rectangular electric pulses with varying amplitudes (2, 3, 4, 5, and 6V) and three different pulse widths in the ratios 1:4, 1:1 and 4:1, i.e., the rectangular pulses having duty cycles 20%, 50% and 80%, respectively, have been used.

Figure 5a shows the POM image obtained at room temperature for **ILLC$_1$(60)** after heating it at an isotropic state and then cooling to a lower temperature in the presence of electric pulse of 3V with 20% duty cycle. Increasing the pulse widths in the ratios 1:4, 1:1 and 4:1 show maltese type crosses with only a slight changes in the droplet morphology (**Fig. 5a–c**). These changes become significant when compared with the images captured after removing the field (**Fig. 5d**).

However, cooling of **ILLC$_1$(60)** from an isotropic state to a lower temperature in the presence of electric pulse of 3V with 50% duty cycle shows nematic droplets of much smaller size and uniform distribution as compared with the one observed for electric pulse of 3V with 20% duty cycle (**Fig. 6a**). To study the effect of field strength on the LC droplet orientation, electric pulses of increasing field strengths and duty cycles in the consecutive steps of 50%, 80% and 20%, respectively, have been applied to the cell. Comparisons show that LC droplet orientation changes for both with increase in the field strength and also with change in the duty cycle. With increase in the field strength particularly for electric pulse of 5V (with duty cycles 50% and 80%), nematics droplets of smaller size get disappeared. These nematic droplets appear again with lowering or removal of the applied electric pulses (**Fig. 6g–i**). It may be due to the changes occurring in **IL** with increasing field strength, which in turn cause the **LC** director orientations to change in droplets surrounded by **IL** as an effect of anchoring.

Further, increasing the field strength above 5V dissociation of **IL** starts in the mixture and is observed as a change in the color of the cell before and after the application of the electric field. In this case, after removal of applied electric field, POM image shows the encapsulation of **LC** droplets in the dissociated **IL** (**Fig. 7**). Behavior of the mixture is re-investigated by applying electric pulses of different field strength and monitoring them though POM.

Observations show significant change in the **LC** droplet orientation with the application of the field as compared to the one observed without field (**Fig. 7 and Fig. 8**). In a dissociated mixture further increase in the field strength and variation in the pulse width upto a certain limit (where the anchoring effect is suppressed) do not make significant changes in the orientation of the **LC** droplets. However, it affects the dissociation process of **IL** which appears as a change in the optical contrasts in the POM images (**Fig. 8 a-l**). As compared with dissociated mixtures (**Fig. 8**), non-dissociated mixtures show that only a small change in the field strength and pulse width is sufficient to change the anchoring condition. As a result, significant changes in the droplet morphology and director orientations were observed before the dissociation of **IL** in the mixtures (**Fig. 6**).

Figure 9 shows the morphological changes observed in the binary mixtures of $\mathbf{LC_2}$ i.e., PCH5 and **IL** by varying the electric field strength and pulse width. For $\mathbf{ILLC_2(80)}$, nematic droplets with uniformity in size, arrangement and **LC** director orientations are observed at 3V. Observed morphology for electric pulses of 3V and 50% duty cycle show uniformly distributed nematic droplets with schlieren textures which also follow a definite pattern of LC director orientations within the droplets (shown in the circled region) (**Fig. 9a**). In the same mixture, enhancement in the duty cycle to 80% (with electric pulse of 3V) results in bipolar droplets having partial ordering of the LC directors within the droplets (shown in the rectangular region) (**Fig. 9b**). Decrease in the duty cycle to 20% show bipolar droplets with increase in droplet size due to coalescence of smaller nematic droplets into the larger one (**Fig. 9c**). Processes of coalescence get affected by change in the field strength because it imposes different anchoring conditions at the surface of the droplets. **Figure 9d** shows LC droplets of intermediate size with uniformity in the arrangement of maltese type of crosses in $\mathbf{ILLC_2(80)}$ when electric pulse of 4V

and 50% duty cycle is applied. When the field is removed or duty cycle is decreased, nematic droplets of comparatively smaller size get coalesced in to the larger one due to the reduced anchoring conditions (**Fig. 9c,e**). Further, electric pulse of 4.5V with 80% duty cycle shows stable and uniform droplets for **ILLC$_2$(90)** (**Fig. 9f**).

Effect of varying field strengths and anchoring conditions on the LC director orientations in the region of *IN* phase coexistence has been discussed by Kedziora et. al. for 6CHBT dissolved in benzene solution.[34] It is described that in the nematic phase i.e., for temperature < T_{IN} when applied electric field is below a critical value, it is not strong enough to turn the LC directors away from the surface of the electrode and molecules get oriented parallel to the electrode surfaces. But, when the applied field is higher than a critical value, electric field rotates the LC director in a direction perpendicular to the electrode surface. However, close to T_{IN} a two phase region with pseudonematic domains in the form of droplets exists. In this case, nematic droplets are surrounded by the isotropic phase where surface effects become negligible. Consequently, even a weaker electric field is sufficient to rotate the LC directors inside a nematic droplet in the direction parallel to the field (i.e., perpendicular to the electrode surface).With decrease in the temperature droplets grow in size and interaction with the aligning surfaces becomes more effective which rotates the LC director in a direction parallel to the electrode surfaces.[33] POM images in the present manuscript show that LC director orientation and droplet randomization is affected significantly with change in the pulse width i.e., duty cycle of the applied voltage. These effects are described in the later portion of the manuscript in the frame of Landau-de Gennes theory (LDG).

For both the nematogens (i.e., 6CHBT and PCH5) investigation on DSC thermograms and POM images show decrease in the onset and endset of *IN* transitions for decreasing

compositions of nematogens in the mixtures. Therefore, *IN* transition range (ΔT) in the mixtures can be optimized by making change in compositions of both the constituents. Noticeably, this optimization also depends on some other factors like isotropic to nematic transition temperature (T_{IN}),[41] applied fields,[33] correlation lengths,[34,35] long and short time-scale dynamics,[35,36] etc. Nematic state in the binary mixtures of nematogens with other mesogens,[14] solvents,[33, 34] polymers,[16] etc. can be achieved either by decreasing the temperature of the mixtures below its isotropic state or by increasing the concentration of nematogenic molecules in the unit volume of the mixtures at constant temperature (but, below the clearing temperature of the nematogen).[34] In such mixtures, transition go through two phase regions with boundary concentrations of nematogens at which (i) first drop of the nematic phase appears and (ii) last drop of the isotropic phase disappears. These two boundary concentrations are determined by constructing the phase diagram using DSC and POM. Transition temperatures data obtained through POM and DSC thermograms have been used frequently to construct the phase diagrams.[14,16, 33, 34] Studies reveal that the phase diagram of *IN* transition *via 'droplet state'* (i.e., the region of coexistence of the isotropic and nematic phases) provides an appropriate information about the critical concentration of nematogens for occurrence of *IN* transition and observed decrease in T_{IN} for decreasing LC concentrations in the mixtures with other materials.[33, 34]

At temperatures slightly above but close to *IN* transitions orientational dynamics of LC molecules gets influenced by the local structures existing in their isotropic phase.[42] Due to short – range orientational ordering of the LC molecules, pseudonematic domains are formed in the isotropic phase and their size increases as the temperature of the mesogen approaches to T_{IN}.[34] This pretransitional phenomena observed in isotropic phase of the mesogen in the vicinity of

nematic phase is interpreted by the Landau-de Gennes theory (LDG).[42] The LDG theory shows that close to *IN* phase transition, isotropic phase is nematically ordered on a distance scale defined by intermolecular correlation length (ξ) which depends strongly on temperature and is usually few degrees below T_{IN}.[42]Correlation length (ξ) is also reported to depend on the LC concentration i.e., the number of LC molecules in the unit volume of the mixtures.[34] Two experimental facts are crucial for concentration dependence of ξ; (i) domain size becomes infinite for transition to nematic phase and (ii) for a two phase regions i.e., for coexistence of *IN* transition domain size become finite and is observed as pseudonematic domains (i.e., droplets) through POM.[34] In the region of coexistence, on a distance scale shorter than ξ, the nematogens form pseudonematic domains with local order parameter $S_L \neq 0$ while it is $S=0$ for a macroscopically isotropic phase.[36] In this case, for an applied electric pulse when field is in ON state, LC molecules experience a torque and get partially aligned ($S \neq 0$) in the direction of the field. But, for an OFF state, removal of the field reestablishes $S=0$ in the LC molecules which were left earlier with $S \neq 0$. Restoration of $S=0$ is described in two time regimes.[35,36] First one is the intradomain relaxation (responsible for the short time scale dynamics) which brings the local order back to its equilibrium but leaves the local director in a direction slightly aligned with the direction of applied field. Another one is the domain randomization which restores the direction of the local directors after having in a long-lived anisotropy and is responsible for long time scale dynamics described by LDG theory.

These investigations confirm the occurrence of nematic droplets in the binary mixtures of both the nematogens (i.e., 6CHBT and PCH5) with phosphonium ionic liquid having [Ntf_2] anion. It suggests that for both the nematogens, **IL** behaves as a less / non – interacting pseudo matrix where dispersion of LCs having a close resemblance with the common droplet

morphologies observed in PDLCs becomes possible. This non – interacting and dispersive behaviour of nematogens in their mixtures with **IL** becomes more clear using FTIR and TGA investigations.

Dispersion studies of LC_1 and LC_2 in IL

The FTIR spectra and TGA thermograms for **LC_1**, **IL** and their mixtures are shown in **Fig. 10**. Various vibrational bands observed in FTIR spectra were identified with the available data[38, 43-48] and are given in **Table 3**. Szaleniec et. al., have made a detailed investigation on the molecular properties of 6CHBT using theoretical FTIR spectra and electrostatic potential distribution (ESP).[38] Our experimental FTIR spectra matches nicely with their theoretical FTIR spectra. As reported for bulk 6CHBT, –N=C=S ligand involves various interactions including C≡N stretching at 2184 cm^{-1}, C=N stretching at 2075 cm^{-1} and –N=C=S stretching at 2125 cm^{-1} which result in a broadened peak in the range 2000 cm^{-1} to 2140 cm^{-1}(**Fig. 10**). The other characteristic peaks are associated with in-plane bending of the NCS group or out-of-plane bending of the aromatic ring at 536 cm^{-1}, out-of-plane bending of the aromatic hydrogen atoms at 828 cm^{-1}, ring breathing C=C stretching at 932 cm^{-1}, scissor deformations of CH_3 and CH_2 groups at 1447 cm^{-1}, CH_2 bending at 1466 cm^{-1}, aromatic ring stretching combined with C=N stretching at 1506 cm^{-1} and various symmetric and asymmetric aliphatic chain stretching in the range 2850 cm^{-1} to 3050 cm^{-1}. The FTIR spectra of **IL** i.e., $[P_{6,6,6,14}][NtF_2]$ show the characteristic vibrations related to Ntf_2 anion at 1059 cm^{-1}, 1137 cm^{-1}, 1195 cm^{-1} and 1378 cm^{-1} alongwith other vibrations related to long aliphatic chain **(Table 3).** Vibrations related to Ntf_2 in the range 1000 cm^{-1} to 1400 cm^{-1} have not shown any change and occur only for mixtures with higher IL contents.

It is important to note from the **Table 3** that the characteristic vibrations which were observed only in 6CHBT or only in $[P_{6,6,6,14}][NtF_2]$ have not shown any significant change in their mixtures. The only exception occurs at 1414 cm^{-1} which is related with CH_3 bending in **IL** molecules. However, the vibrational bands related with stretching / bending of aliphatic chains which were observed in both 6CHBT and in $[P_{6,6,6,14}][NtF_2]$ show small shifts due to overlapping of corresponding vibrations in their mixtures. In the **Fig. 10a, ILLC$_1$(80)** and **ILLC$_1$(50)** show some additional vibrations below 1000 cm^{-1} which were not observed either in **LC$_1$** or in **ILLC$_1$(90)** but they were found in **IL**. Absence of an appreciable shift in the characteristic vibrations of both the constituents suggests a non – interacting behaviour between **LC$_1$** and **IL** in their mixtures.

The TGA thermograms for pure **LC$_1$**, **IL** and for their mixtures are shown in **Fig. 10b**. It shows that the decomposition temperatures for pure **LC$_1$** and **IL** are at ~300 ^{0}C and ~430 ^{0}C, respectively. Different mixtures show a two step decomposition in which weight loss associated with each step decomposition depends strongly on the composition of respective constituents. Moreover, for mixtures, both, the first and second step decompositions are observed much closer to the decomposition temperatures of pure **LC$_1$** (~ 300 ^{0}C) and **IL** (~ 430 ^{0}C). It shows that the thermal stability of both the constituents remains intact separately in their mixtures. Similar thermogravimetric observations were also found for the various mixtures of **LC$_2$** and **IL** with decomposition of **LC$_2$** at ~ 270 ^{0}C.

Summary and conclusions

In the present work, we have observed the formation of nematic droplets at room temperature in various binary mixtures of the nematic liquid crystals, 6CHBT and PCH5, with phosphonium ionic liquid $[P_{6,6,6,14}][Ntf_2]$. These mixtures have been investigated using DSC, POM, FTIR and TGA techniques.

The thermal and morphological investigations on these mixtures show that for both the LCs, peak value of T_{IN} decrease drastically as compared to pure LCs. In fact, T_{IN} is decreased, respectively, by 7.5 ^{0}C for **ILLC$_1$(50)**, 18.6 ^{0}C for **ILLC$_2$(90)** and 35.4 ^{0}C for **ILLC$_2$(80)**. Inspite of the fact that *IN* transition temperature range is very narrow for most of the binary mixture, POM images for various combinations show the occurrence of stable nematic droplets over a wide temperature range ~20 ^{0}C (i.e. from ~16 ^{0}C to ~36 ^{0}C) with change in the composition of LCs in their mixtures. Moreover, change in the LC droplets size and director orientations inside these droplets have been observed with application of rectangular electric pulses. Thus, by tailoring the compositions of various mixtures and applied field strengths with a swift in anchoring condition, uniform nematic droplets in a desired temperature range and size can be obtained. The FTIR investigations for various binary mixtures show only a slight change in some of the vibrational bands of **LC$_1$** due to overlapping with the corresponding **IL** vibrations. The TGA investigation of various binary mixtures does not show significant change in the decomposition temperature of both the **LCs** (i.e., 6CHBT and PCH5) in $[P_{6,6,6,14}][Ntf_2]$. The weight loss associated with each decomposition step depends strongly on the composition of their respective constituents i.e., **LCs** and **IL**. It shows that both the constituents remain nearly immiscible in their mixtures. Thus, the FTIR and TGA analyses combined with the thermal and morphological studies for various binary mixtures confirm that both the LCs behave as a

dispersed (entrapped) material in the non – interacting pseudo matrix formed by PIL having [Ntf_2] anion.

In brief, dispersions of nematic droplets near room temperatures have been observed for both the 6CHBT and PCH5 in their binary mixtures with [$P_{6,6,6,14}$][Ntf_2]. These nematic droplets resemble much with the common droplet morphologies observed in PDLCs. Even small changes in applied electric field or pulse width have significant effects on the LC droplet size and director orientations within the droplets. It demonstrates strong potential for these kinds of mixtures alongwith some other mesogens and ionic solvents in PDLC based device applications with improved performance and eco –friendly behaviour.

References

1 L. Vicari, *Optical Applications of Liquid Crystals*, IOP Publishing, 2003.

2 D. K. Yang and S. T. Wu, *Fundamentals of Liquid Crystal Devices*, John Wiley & Sons, 2006.

3 P. S. Drzaic, *Liquid Crystal Dispersions*, World Scientific, Singapore, 1995.

4 P. Pasini, C. Zannoni and S. Zumer, *Computer Simulations of Liquid Crystals and Polymers*, Nato Science Series, Kluwer Academic Publishers, Netherlands, 2003.

5 F. Simoni, *Nonlinear Optical Properties of Liquid Crystals and Polymer Dispersed Liquid Crystals*, World Scientific, Singapore, 1997.

6 D. A. Higgins, Probing the Mesoscopic Chemical and Physical Properties of Polymer Dispersed Liquid Crystals, *Adv. Mater.*, 2000, **12**, 251 – 264.

7 S. Singh, J. K. Srivastava and R. K. Singh, *Polymer Dispersed Liquid Crystals, in, Liquid Crystalline Polymers: Advances and Applications*, eds., V.K. Thakur and M.R. Kessler, Springer Verlag, 2015.

8 M. M. Dzhons, S. A. Bulgakova, I. A. Pantyukhina and I. A. Kazantzeva, Effects of Chemical Structure and Composition of the Polymer Matrix on the Morphology and Electro-Optical Performance of Polymer Dispersed Liquid Crystal Films, *Liq. Cryst.*, 2011**, 38**, 1263 – 1268.

9 N.H. Park, S.C. Noh, P. Nayek, M.H. Lee, M.S. Kim, L.C. Chien, J.H. Lee, B. K. Kim and S.H. Lee, Optically isotropic liquid crystal mixtures and their application to high – performance liquid crystal devices, *Liq.Cryst.*, 2015, **4**, 530 – 536.

10 E. Perju, E. Paslaru and L. Martin, Polymer dispersed liquid crystal composites for bio-applications: thermotropic surface and optical properties, *Liq. Cryst.*, 2015, **42**, 370 – 382.

11 P. Song, Y. Gao, F. Wang, L. Zhang, H. Xie, Z. Yang and H. Yang, Studies on the eoectro-optical and the light scattering properties of PDLC films with the size gradient of the LC droplets, *Liq. Cryst.*, 2015, **42**, 390 – 396.

12 G. B. Hadjichristov, Y. G. Marinov and A. G. Petrov, Linear Size Gradient Single Layers of Polymer Dispersed Liquid Crystal Micrometer Sized Droplets for Diffractive Optics, *Opt. Mater.*, 2009, **31**, 1578-1585.

13 P. Formentin, R. Palacios, J. F. Borrull, J. Pallares and L. F. Marsal, Polymer Dispersed Liquid Crystal based on E7: Morphology and Characterization, *Synth. Metals*, 2008, **158**, 1004 – 1008.

14 S.L. Srivastava and R. Dhar, Thermodynamic study of binary mixtures of liquid crystals cholesteryl myristate and dodecyloxybenzoic acid, *Mol. Crys. Liq. Crys.*, 2001, **366**, 79-90.

15 E. R. Soule, N. M. Abukhdeir and A. D. Rey, Thermodynamics, Transition Dynamics and Texturing in Polymer Dispersed Liquid Crystals with Mesogens Exhibiting a Direct Isotropic / Smectic A Transition, *Macromolecules*, 2009, **42**, 9486 – 9497.

16 J. K. Srivastava, R. K. Singh, R. Dhar and S. Singh, Phase Diagrams and Morphology of Polymer – Dispersed Liquid Crystals: An Analysis, *Liq. Cryst.*, 2012, **39**, 1402 – 1413.

17 J.Y. Kim, H.Y. Woo, J.W. Baek, T. W. Kim, E. A. Song, S.C. Park and D.W. Ihm, Polymer Dispersed Liquid Crystal Devices using Highly Conducting Polymers as Electrodes, *Appl. Phys. Lett.*, 2008, **92**, 183301.

18 J. Zou and J. Fang, Adhesive Polymer Dispersed Liquid Crystal Films, *J. Mater. Chem.*, 2011, **21**, 9149 – 9153.

19 N. Kumano, T. Seki, M. Ishii, H. Nakamura, T. Umemura and Y. Takeoka, Multicolor Polymer Dispersed Liquid Crystals, *Adv. Mater.*, 2011, **23**, 884 – 888.

20 O. Yaroshchuk and Y. Reznikov, Photoalignment of Liquid Crystals: Basics and Current Trends, *J. Mater. Chem.*, 2012, **22**, 286 – 300.

21 F. Merola, S. Grilli, S. Coppola, V. Vespini, S. D. Nicola, P. Maddalena, C. Carfagna and P. Ferraro, Reversible Fragmentation and Self Assembling of Nematic Liquid Crystal Droplets on Functionalized Pyroelectric Substrates, *Adv. Funct. Mater.*, 2012, **22**, 3267 – 3272.

22 T. Kato, Self Assembly of Phase Segregated Liquid Crystal Structures, *Science*, 2002, **295**, 2414 – 2418.

23 K. Binnemans, Ionic Liquid Crystals, *Chem. Rev.*, 2005, **105**, 4148 – 4204.

24 K.V. Axenov and S. Laschat, Thermotropic Ionic Liquid Crystals, *Materials*, 2011, **4**, 206 – 259.

25 W. Li, J. Zhang, B. Li, M. Zhang and L. Wu, Branched Quaternary Ammonium Amphiphiles: Nematic Ionic Liquid Crystals near Room Temperature, *Chem. Commun.*, 2009**,** 5269 – 5271.

26 D. Cupelli, F.P. Nicoletta, S. Manfredi, M. Vivacqua, P. Formoso, G. De Filpo and G. Chidichimo, Self Adjusting Smart Windows based on Polymer Dispersed Liquid Crystals, *Solar Ene. Mat. & Solar Cells*, 2009, **93**, 2008 – 2012.

27 F.P. Nicoletta, D. Cupelli, G. De Filpo, M. Macchione and G. Chidichimo, Quasilinear Electro Optical Response in a Polymer Dispersed Nematic Liquid Crystal, *Appl. Phys. Lett.*, 2000, **77**, 3689 – 3691.

28 D. Cupelli, F. P. Nicoletta, G. De Filpo, P. Formoso and G. Chidichimo, Reverse Mode Operation Polymer Dispersed Liquid Crystal with a Positive Dielectric Anisotropy Liquid Crystal, *Poly. Sci.: Part B: Poly. Phys.*, 2011, **49**, 257 – 262.

29 H. Ren, S.H. Lee and S.T. Wu, Reconfigurable Liquid Crystal Droplets using a Dielectric Force, *Appl. Phys. Lett.*, 2009, **95**, 241108.

30 S.K. Fan, C.P. Chiu and J. W. Lin, Electrowetting on Polymer Dispersed Liquid Crystal, *Appl. Phys. Lett.*, 2009, **94**, 164109.

31 C.V. Yelamaggad, M. Mathews, U.S. Hiremath, D.S.S. Rao and S.K. Prasad, Self-organization of mesomeric–ionic hybrid heterocycles into liquid crystal phases: a new class of polar mesogens, *Chem. Commun.*, 2005, 1552-1554

32 K. Goossens, P. Nockemann, K. Driesen, B. Goderis, C.G.Walrand, K.V. Hecke, L.V. Meervelt, E. Pouzet, K. Binnemans and T. Cardinaels, Imidazolium Ionic Liquid Crystals with Pendant Mesogenic Groups, *Chem. Mater.*, 2008, **20**, 157–168.

33 N. Tomasovicova, P. Kopcansky, M. Koneracka, L. Tomco, V. Zavisova, M. Timko, N. Eber, K. F. Csorba, T. T. Katona, A. Vajda and J. Jadzyn, The Structural Transitions in 6CHBT based Ferronematic Droplets, *J. Phys.: Condense Matter*, 2008, **20**, 204123.

34 P. Kedziora, J. Jadzyn and L. Hellemans, Dynamics of the Nonlinear Dielectric Properties of a Nematogenic Compound Dissolved in a Nonpolar Medium, *Phys. Rev. E*, 2002, **66**, 021709.

35 J. Li, H. Cang, H.C.; Andersen and M.D. Fayer, A Mode Coupling Theory Description of the Short and Long Time Dynamics of Nematogens in the Isotropic Phase, *J. Chem. Phys.*, 2006, **124**, 014902.

36 J. Li, I. Wang and M.D. Fayer, Three Homeotropically Aligned Nematic Liquid Crystals: Comparison of Ultrafast to Slow Time Scale Dynamics, *J. Chem. Phys.*, 2006, **124**, 044906.

37 S. Ueda, J. Kagimoto, T. Ichikawa, T. Kato and H. Ohno, Anisotropic Proton Conductive Materials formed by the Self Organization of Phosphonium type Zwitterions, *Adv. Mater.*, 2011, **23**, 3071 – 3074.

38 M. Szaleniec, R.T. Sobieraj and W. Witko, Theoretical Study of 1 – (4 – hecylclohexyl) – 4 – isothiocyanatobenzene: Molecular Properties and Spectral Characteristics, *J. Mol. Model*, 2009, **15,** 935 – 943.

39 W. Witko, A. M. Padol and P. M. Zielinski, Multiple melting phenomena in low mass mesogenic compound, *Phase Transitions*, 2007, **80**, 717–724.

40 F.U. Shuren and C. Taoyung, Multiple melting in Nylon 1010, *Poly. Commun.*, 1983, **2**, 145-151.

41 P. Kopcansky, M. Koneracka, M. Timko, I. Potocova, L. Tomco, N. Tomasovicova, V. Zavisova and J. Jadzyn, The structural transitions in ferronematics and ferronematic droplets, *J. Magn. Magn. Mater.*, 2006, 300,75–78.

42 P.G. de Gennes, Physics of Liquid Crystals, Oxford University Press, Oxford, 1974.

43 D.S. Jacob, S. Makhluf, I. Brukental, R. Lavi, L.A. Solovyov, I. Felner, I. Nowik, R. Persky, H.E. Gottlieb and A. Gedanken, Sonochemical Synthesis and Characterization of $Ni(C_4H_6N_2)_6(PF_6)_2$, $Fe(C_4H_6N_2)_6(BF_4)_2$ and $Ni(C_4H_6N_2)_6(BF_4)_2$ in 1–butyl–3–

methylimidazole with hexafluorophosphate and tetrafluoroborate, *Eur. J. Inorg. Chem.*, 2005, 2669 – 2677.

44 R. Verma, R. Dhar, M.C. Rath, S.K. Sarkar, V.K. Wadhawan, R. Dabrowski and M.B. Tykarska, Optimization of the Display Parameters of a Room Temperature Nematic Material (6CHBT) by using Electron Beam Irradiation, *J. Disp. Tech.*, 2010, **6**, 8 – 13.

45 M.P. Singh, R.K. Singh and S. Chandra, Studies on Imidazolium based Ionic Liquids having a Large Anion Confined in a Nanoporous Silica Gel Matrix, *J. Phys. Chem. B*, 2011, **115**, 7505 – 7514.

46 Y. Mochizuki and K. Sugawara, Removal of Organic Sulfur from Hydrocarbon Resources using Ionic Liquids, *Energy & Fuels*, 2008, **22**, 3303 – 3307.

47 J.C. Lassegues, J. Grondin, D. Cavagnat and P. Johansson, New Interpretation of CH Stretching Vibrations in Imidazolium Based Ionic Liquids, *J. Phys. Chem. A*, 2009, **113**, 6419 – 6421.

48 S.B. Dhiman, G.S. Goff, W. Runde, J.A. Laverne, Gamma and heavy ion radiolysis of ionic liquids: A comparative study, *J. Nuclear Mater.*, 2014, **453**, 182–187.

Figure captions:

Fig. 1 DSC thermograms during second cooling step from 110 ^{0}C to -40 ^{0}C for various mixtures of (a) **LC_1** and (b) **LC_2** with **IL** and their pure constituents. Insets of the figures show enlarged views of the respective regions.

Fig. 2 POM images for (a) **$ILLC_1(90)$**, (b) **$ILLC_1(75)$**, (c) **$ILLC_1(60)$** at 28 ^{0}C; and for (d) **$ILLC_1(50)$** at 20 ^{0}C.

Fig. 3 Evolution of the droplet morphology for **$ILLC_2(90)$** at (a) 40 ^{0}C, (b) 37 ^{0}C, (c) 35 ^{0}C, (d) 34 ^{0}C, (e) 33 ^{0}C and (f) 28 ^{0}C showing the coalescence of nematic droplets in macroscopic domains.

Fig. 4 POM images for **$ILLC_2(80)$**: (a), (b) and (c); for **$ILLC_2(75)$**: (d), (e) and (f). During cooling from an isotropic state to 28 ^{0}C (a) and (d); to 10 ^{0}C (b) and (e); and during heating from an already cooled state at lower temperature to 28 ^{0}C (c) and (f).

Fig. 5 POM images for **$ILLC_1(60)$** captured at room temperature after cooling from an isotropic state in the presence of rectangular electric pulse of 3V with the duty cycle (a) 20%, (b) 50%, (c) 80% and (d) after removal of the field.

Fig. 6 POM images for **$ILLC_1(60)$** using electric pulses of different field strengths. Images are captured after cooling the mixture to room temperature from an isotropic state in the presence of rectangular electric pulse of 3V with duty cycle 50%.

Fig. 7 POM images at room temperature for **$ILLC_1(60)$** after removing the electric pulse of 6V, applied earlier to the mixture.

Fig. 8 POM images for **$ILLC_1(60)$** using electric pulses of different field strengths. Images are captured at room temperature using the cell on which electric pulses up to 6.0V have already been applied.

Fig. 9 POM images (a-e) for **$ILLC_2(80)$** and (f) for **$ILLC_2(90)$**. Electric pulses of different field strengths 3V with duty cycle (a) 50%, (b) 80%, (c) 20% (d) 4V with duty cycle 50%, (e) no field and (f) 4.5V with duty cycle 80% have been used to capture the respective photographs.

Fig. 10 (a) FTIR spectra and (b) TGA thermogram for **LC_1**, **IL** and their various mixtures.

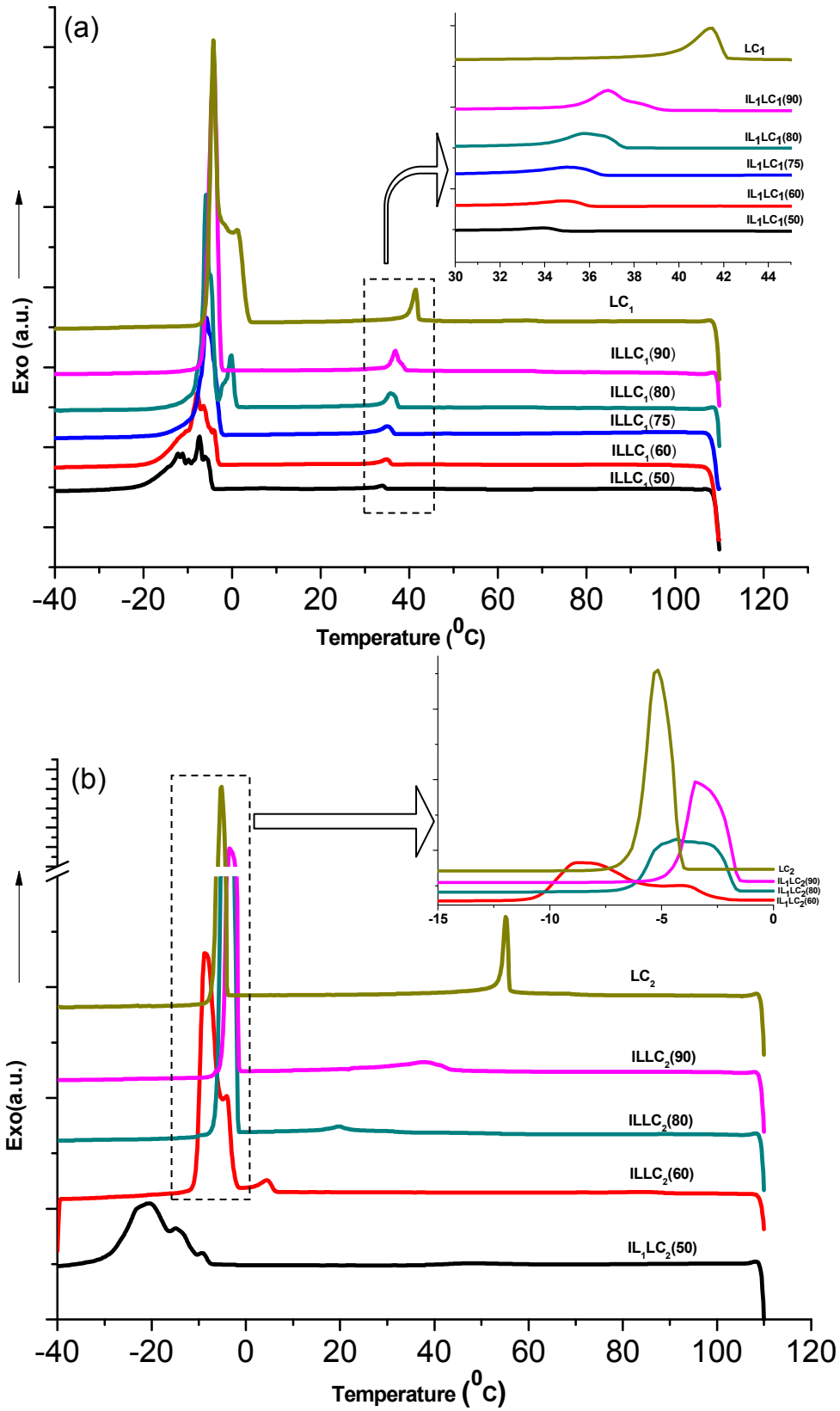

Fig. 1 DSC thermograms during second cooling step from 110 ^{0}C to -40 ^{0}C for various mixtures of (a) **LC_1** and (b) **LC_2** with **IL** and their pure constituents. Insets of the figures show enlarged views of the respective regions.

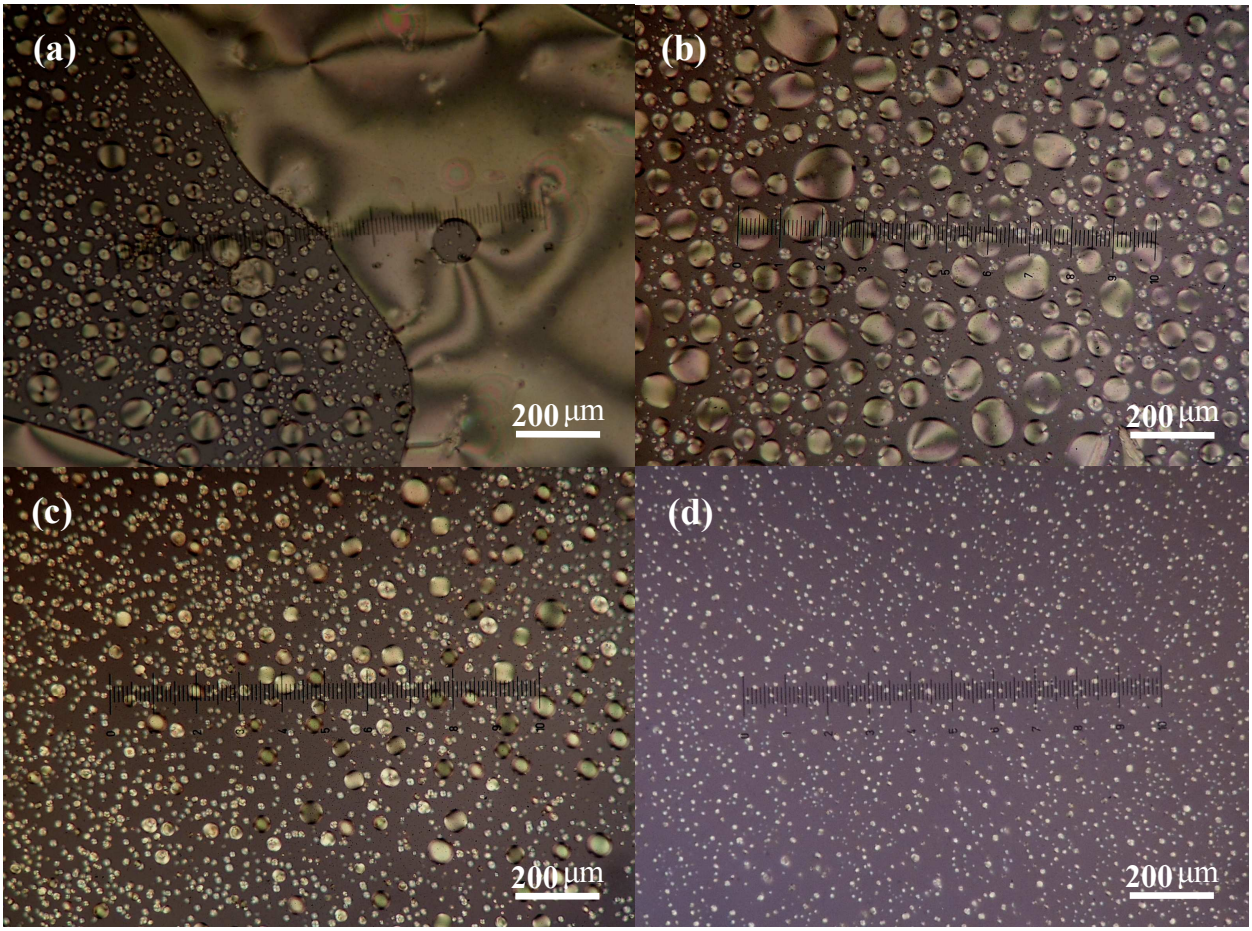

Fig. 2 POM images for (a) **ILLC$_1$(90)**, (b) **ILLC$_1$(75)**, (c) **ILLC$_1$(60)** at 28 ^{0}C; and for (d) **ILLC$_1$(50)** at 20 ^{0}C.

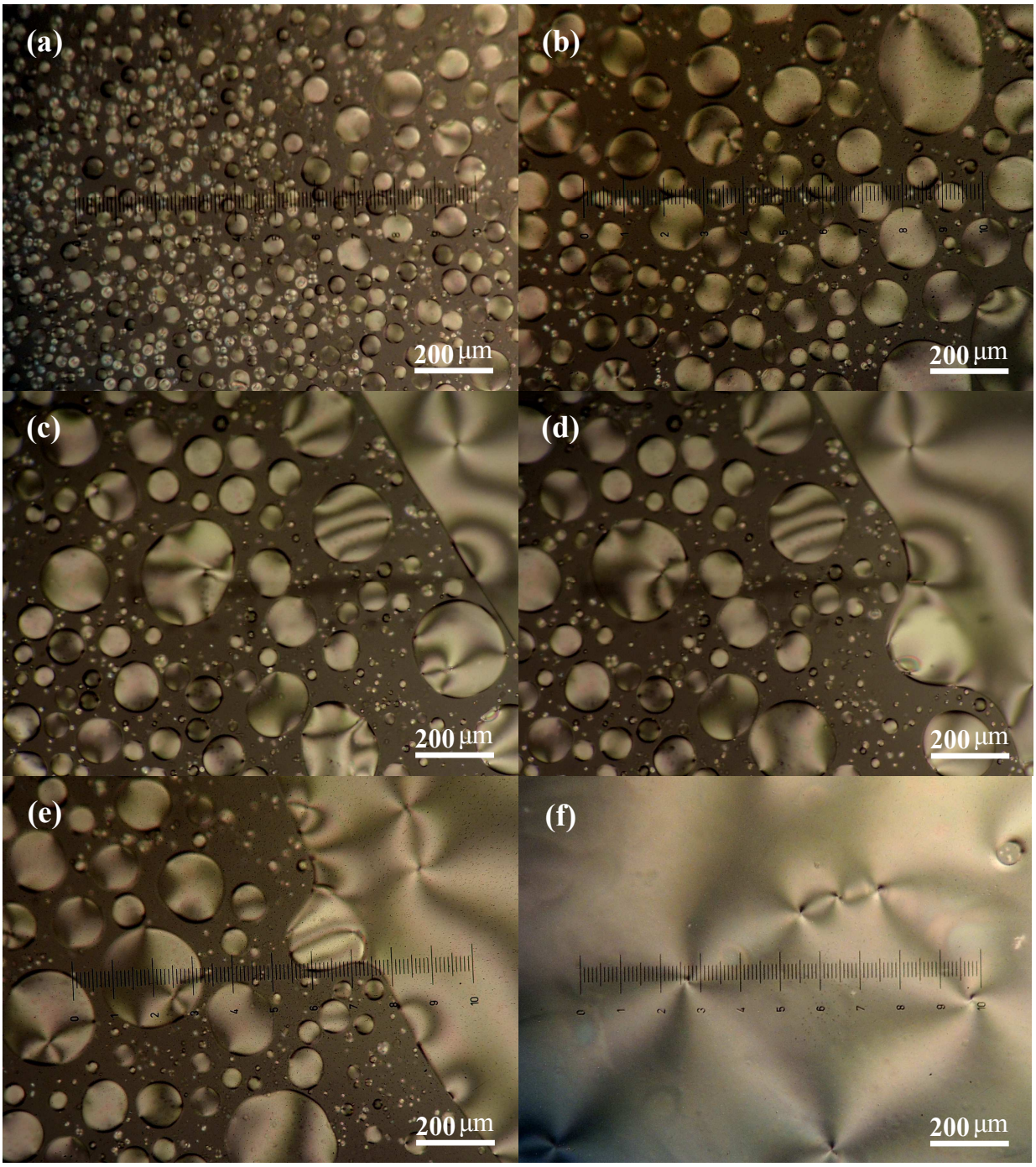

Fig. 3 Evolution of the droplet morphology for **ILLC$_2$(90)** at (a) 40 ^{0}C, (b) 37 ^{0}C, (c) 35 ^{0}C, (d) 34 ^{0}C, (e) 33 ^{0}C and (f) 28 ^{0}C showing the coalescence of nematic droplets in macroscopic domains.

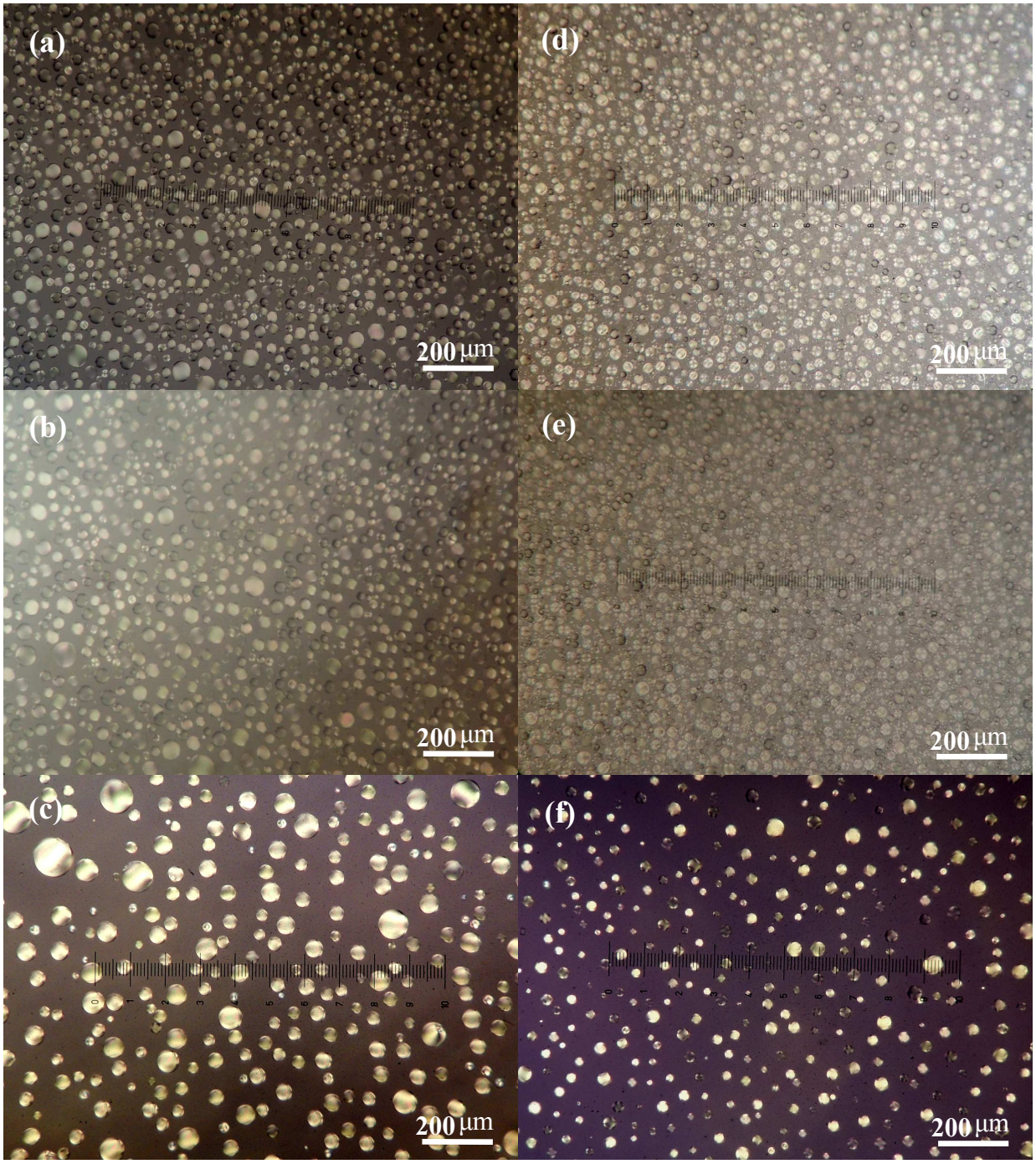

Fig. 4 POM images for **ILLC$_2$(80)**: (a), (b) and (c); for **ILLC$_2$(75)**: (d), (e) and (f). During cooling from an isotropic state to 28 ^{0}C (a) and (d); to 10 ^{0}C (b) and (e); and during heating from an already cooled state at lower temperature to 28 ^{0}C (c) and (f).

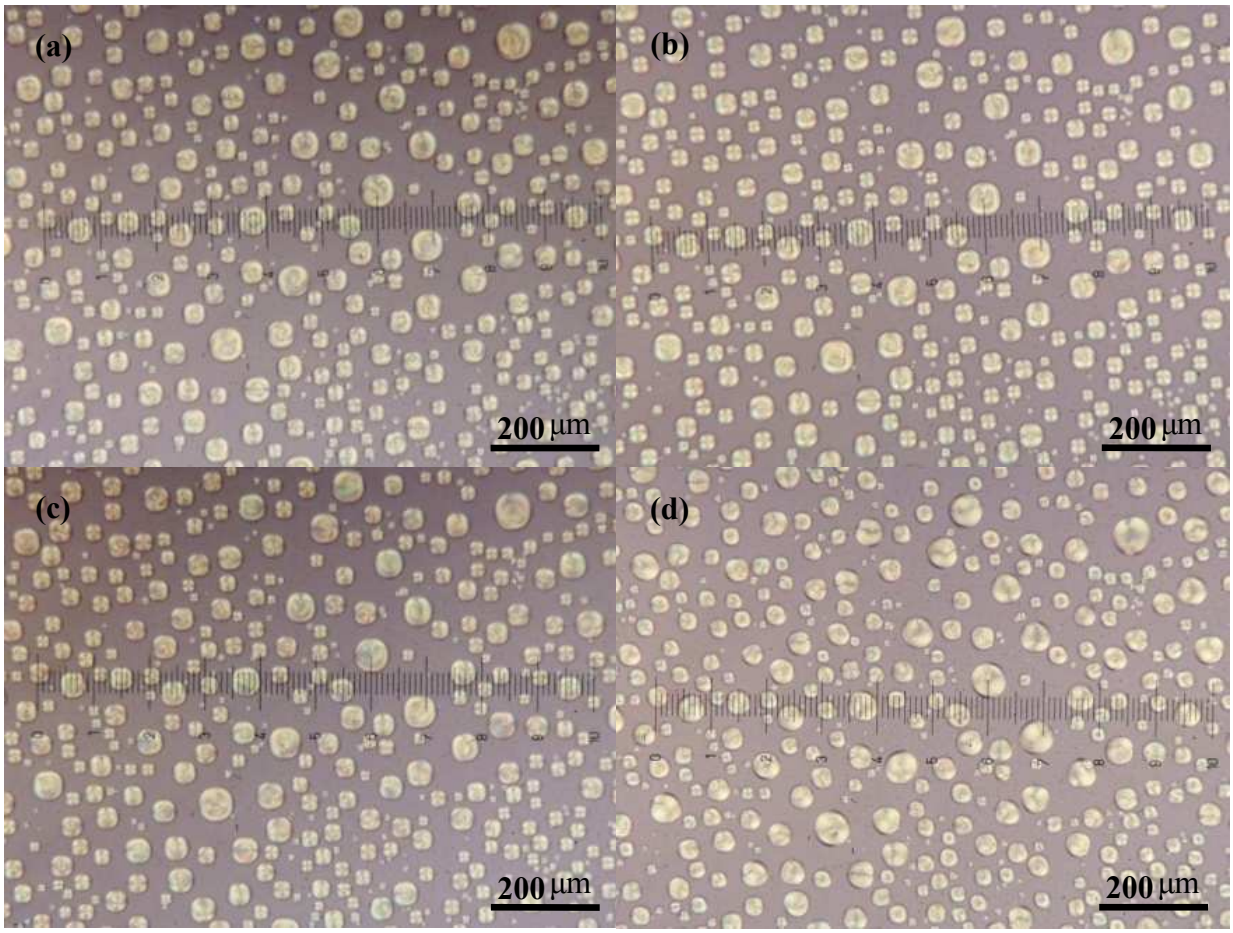

Fig. 5 POM images for **ILLC$_1$(60)** captured at room temperature after cooling from an isotropic state in the presence of rectangular electric pulse of 3V with the duty cycle (a) 20%, (b) 50%, (c) 80% and (d) after removal of the field.

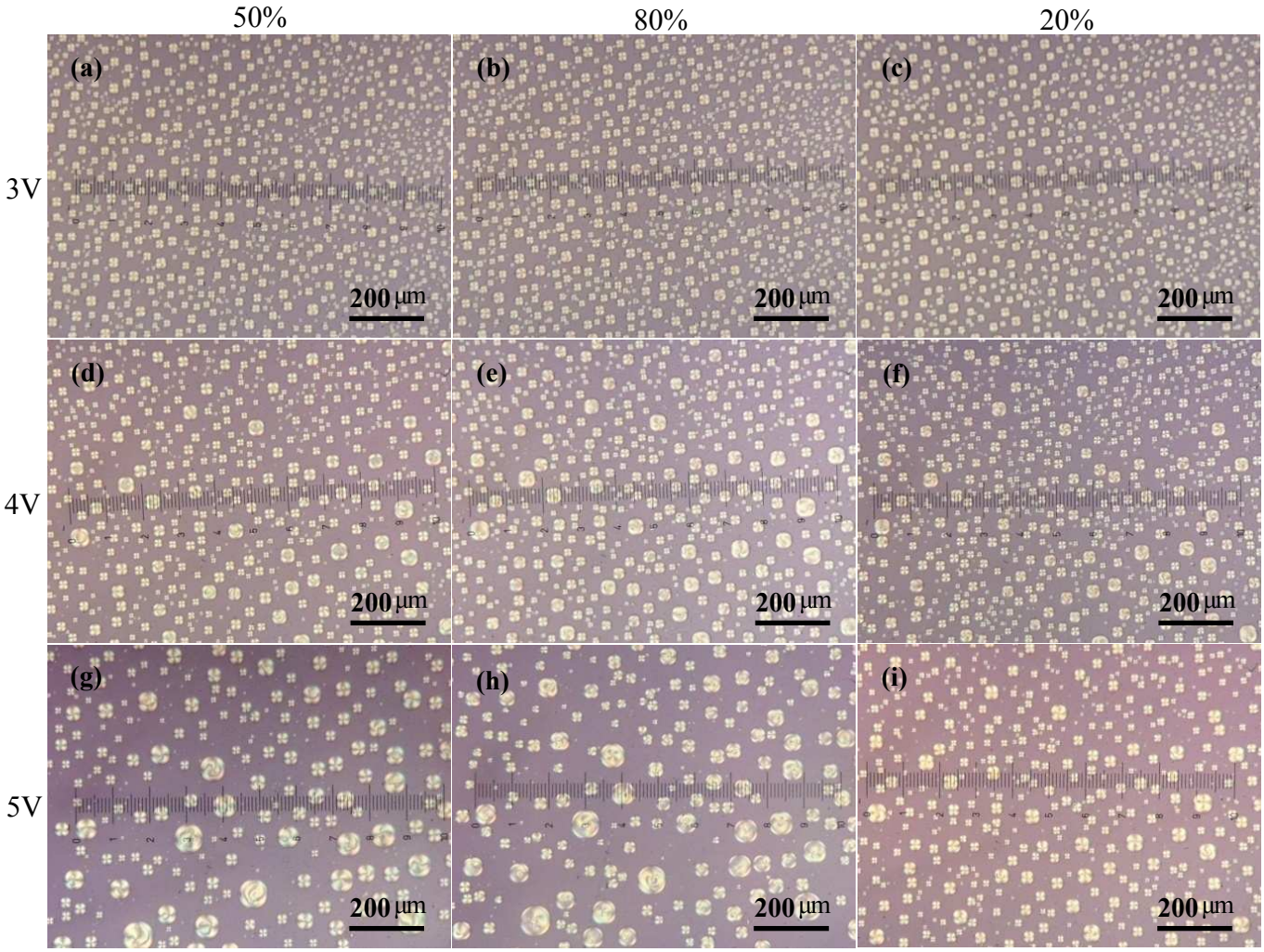

Fig. 6 POM images for **ILLC$_1$(60)** using electric pulses of different field strengths. Images are captured after cooling the mixture to room temperature from an isotropic state in the presence of rectangular electric pulse of 3V with duty cycle 50%.

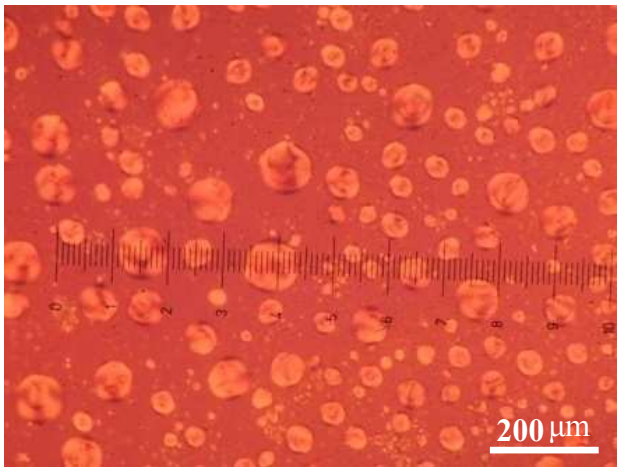

Fig. 7 POM images at room temperature for **ILLC$_1$(60)** after removing the electric pulse of 6V, applied earlier to the mixture.

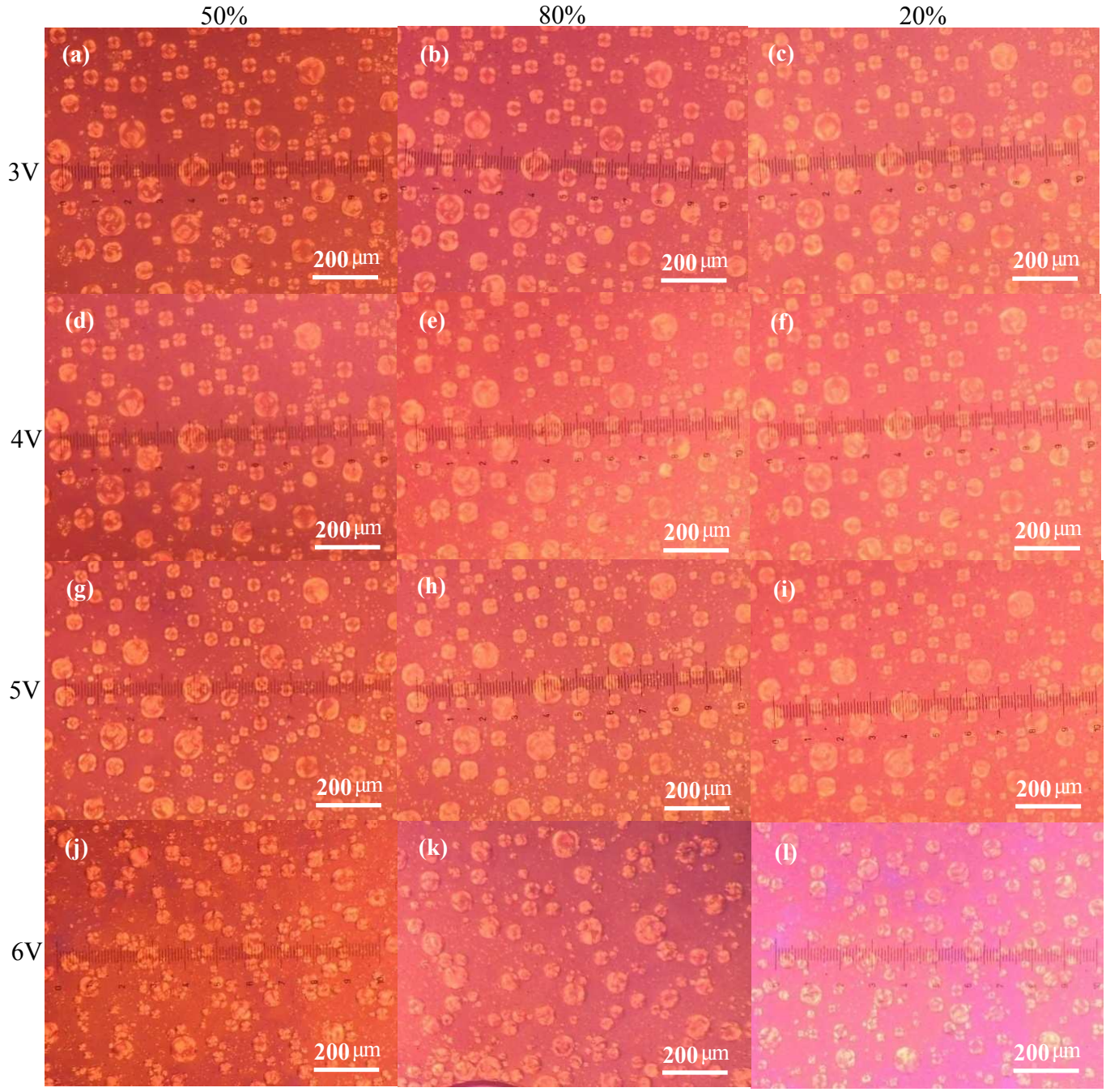

Fig. 8 POM images for **ILLC$_1$(60)** using electric pulses of different field strengths. Images are captured at room temperature using the cell on which electric pulses up to 6.0V have already been applied.

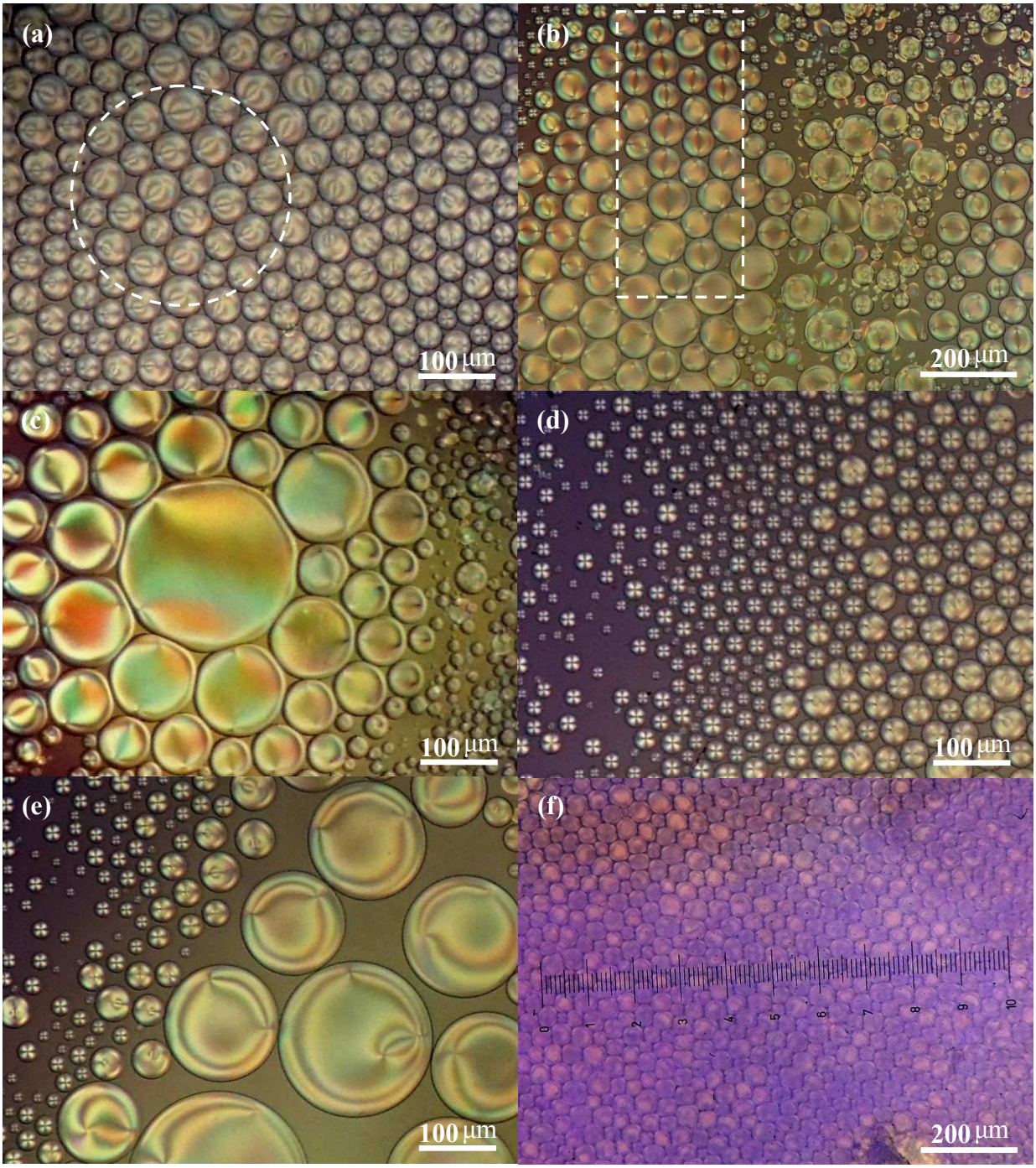

Fig. 9 POM images (a-e) for **ILLC$_2$(80)** and (f) for **ILLC$_2$(90)**. Electric pulses of different field strengths 3V with duty cycle (a) 50%, (b) 80%, (c) 20% (d) 4V with duty cycle 50%, (e) no field and (f) 4.5V with duty cycle 80% have been used to capture the respective photographs.

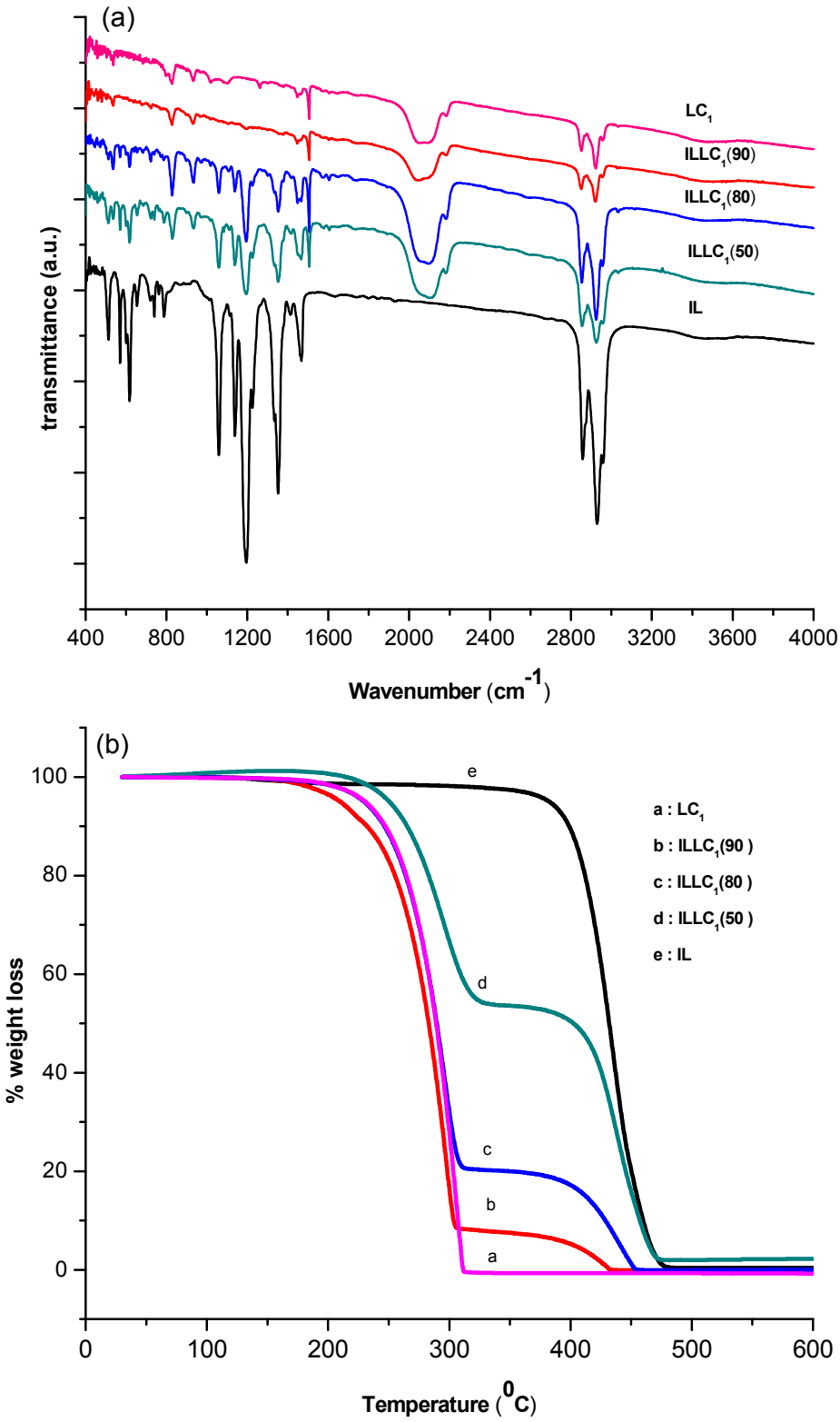

Fig. 10 (a) FTIR spectra and (b) TGA thermogram for **LC_1**, **IL** and their various mixtures.

Table 1 Abbreviation for various binary mixtures of NLCs and PIL. $[P_{6,6,6,14}][Ntf_2]$ = IL, 6CHBT = LC_1 and PCH5 = LC_2

Variation of LCs in IL (by wt%)	IL	
	LC_1	LC_2
90	**$ILLC_1(90)$**	**$ILLC_2(90)$**
80	**$ILLC_1(80)$**	**$ILLC_2(80)$**
75	**$ILLC_1(75)$**	**$ILLC_2(75)$**
60	**$ILLC_1(60)$**	**$ILLC_2(60)$**
50	**$ILLC_1(50)$**	**$ILLC_2(50)$**

Table 2 Thermal investigation of pure LCs and their mixtures with IL for different compositions (by wt%) observed in cooling cycle of DSC.

Mixtures	T_{Cr}	ΔH_{Cr}	T_{IN}	ΔH_{IN}	$T_{IN-onset}$	$T_{IN-endset}$	ΔT_{IN}
LC_1	-3.8	46.94	41.6	2.28	42.3	39.8	1.3
$ILLC_1(90)$	-3.7	42.16	36.9	2.89	38.5	35.2	1.7
$ILLC_1(80)$	-3.6	22.10	35.8	2.41	37.8	33.8	2.4
$ILLC_1(75)$	-5.7	29.59	35.1	2.06	36.8	32.0	2.9
$ILLC_1(60)$	-3.0	23.94	34.9	0.82	36.2	32.2	2.3
$ILLC_1(50)$	-7.2	19.44	34.1	0.49	35.0	31.5	2.0
LC_2	-5.2	66.10	55.3	4.18	56.1	54.0	1.2
$ILLC_2(90)$	-3.4	58.05	36.7	2.71	43.9	32.6	8.4
$ILLC_2(80)$	-4.3	50.00	19.9	0.7	22.5	16.2	3.4
$ILLC_2(60)$	-8.6	36.53	---	---	---	---	---
$ILLC_2(50)$	-20.4	29.60	---	---	---	---	---

T_{Cr} : crystallization transition temperature, ΔH_{Cr} : enthalpy of crystallization, T_{IN} : isotropic to nematic transition temperatures, ΔH_{IN} : enthalpy of IN transition, $T_{IN-onset}$ and $T_{IN-endset}$: onset and endset of IN transition, ΔT_{IN} : peak width of IN transition.

Table 3 IR vibrational bands (cm^{-1}) for various mixtures of **LC_1** and **IL.**

Assignment	Vibrational bands (cm^{-1})				
	LC_1	**$ILLC_1(90)$**	**$ILLC_1(80)$**	**$ILLC_1(50)$**	**IL**
C-H stretching of the aliphatic chain	3033	3033	3033	3033	---
C – H stretching in alkyl chain	2958	2958	2958	2959	2960
Asymmetric C–H stretching in cyclohexane and CH_2 groups of nhexane	2922	2922	2924	2924	2929
C – H stretching in alkyl chains	2851	2852	2854	2855	2859
C≡N stretching	2184	2184	2184	2184	---
C=N stretching in the NCS ligand and – N=C=S stretching at 2125 cm^{-1}	2000 -2140	2000 -2140	200 -2140	2000 -2140	---
Aromatic ring stretching combined with C=N stretching	1506	1506	1506	1506	---
CH_2 bending	1466	1467	1467	1468	1468
Scissor deformations of CH_3 and CH_2 groups	1447	1447	1447	1447	---
CH_3 bending	---	---	1417	1417	1414
Ntf_2 related vibrations of IL in the range 1000 cm^{-1} to 1400 cm^{-1}	---	---	1378	1378	1378
	---	1195	1195	1195	1195
	---	---	1137	1137	1137
	---	---	1059	1059	1059
Ring breathing C=C stretching	934	934	934	934	---
Out-of-plane bending of the aromatic hydrogen atoms	828	828	828	828	---
Out of plane C-H bending	---	720	720	720	720
In-plane bending of the NCS group or out-of-plane bending of the aromatic ring	536	536	536	536	---